Monthly Notices of the ROYAL ASTRONOMICAL SOCIETY
MNRAS **446,** 3404–3415 (2015) doi:10.1093/mnras/stu2176

High-altitude meteors and meteoroid fragmentation observed at the Jicamarca Radio Observatory

B. Gao and J. D. Mathews★
Radar Space Sciences Lab, Pennsylvania State University, University Park, PA 16802, USA

Accepted 2014 October 13. Received 2014 October 12; in original form 2014 February 09

ABSTRACT

Modern high-power, large-aperture (HPLA) radars have been used in a variety of investigations including the investigation of meteoroid fragmentation. The identification of fragmentation has been based on a detailed interpretation, based on radio science, of head- and trail-echo properties. We now extend the discussion of fragmenting meteoroids to include apparent high-altitude (130–180 km) meteors observed at the Jicamarca Radio Observatory (JRO). While there have been a few reports of high-altitude meteors observed both optically and with radar, the meteor radar community has remained sceptical, with suspicions of antenna side-lobe contamination being the most commonly raised objection. We report results from two sets of meteor observations carried out at JRO in 2010 April. Our findings include meteoroid fragmentation results that are similar to those from the Arecibo VHF radar. These findings lead to the conclusions that fragmentation is not only observed at the JRO but that **k**⊥**B** scattering adds an interesting additional radio science dimension to the issue. We also report on apparent high-altitude meteor events that, if ultimately confirmed, offer insight into sputtering as a source of the meteor ionization, and perhaps indicate the unique importance of magnetic field geometry in these head-echo observations. Also, new, apparently high-altitude transient events, likely related to the meteoroid flux, have been identified. In presenting these results, we note our careful calibration of the JRO radar, utilizing satellite returns in order to largely, if not totally, exclude side-lobe contamination and other possible error sources, as reported in our companion paper.

Key words: techniques: radar astronomy – meteorites – meteors – meteoroids.

1 INTRODUCTION

Arguably, the age of high-power, large-aperture (HPLA) radar studies of meteors began at the Jicamarca Radio Observatory (JRO) when Chapin & Kudeki (1994b) presented striking figures (see their figs 3 and 4) showing not only meteor head-echoes (Mathews et al. 1997; Mathews 2004) but also what are now known as range-spread trail-echoes (RSTEs; Zhou et al. 1998; Zhou, Mathews & Nakamura 2001; Malhotra, Mathews & Urbina 2007a; Malhotra, Mathews & Urbina 2007b; Malhotra, Mathews & Ray 2009). What distinguished the 50-MHz JRO observations from the much earlier HF/VHF radar observations of meteors was, and still is, that the aperture is large, with the entire central beam size of $\sim 2^\circ$ or less depending on the transmit/receive configuration (Malhotra et al. 2007b). The combination of high power (>1 MW) and large aperture renders the JRO radar and other similarly configured radars very sensitive to meteors. The term 'HPLA radar' was introduced by Pellinen-Wannberg (2001) to distinguish the 'classical' high-frequency low-power, small-aperture (LPSA) meteor radar system (McKinley 1961) from the much more sensitive but relatively narrow-beam, vertical- or near-vertical-looking large radar systems. While various manifestations of RSTEs are seen at other radars away from the geomagnetic equator (Zhou et al. 2001; Mathews et al. 2010), the long-lived characteristic of those seen at the JRO radar **k**⊥**B** locus points to the importance of the radio science details of the scattering process (Malhotra et al. 2007a,b). An additional issue is that of meteoroid flaring and fragmentation (Briczinski, Mathews & Meisel 2009; Mathews et al. 2010), which we address when we review the JRO results. A brief history of meteor radar is given by Mathews (2004) and by Baggaley (2009), who give historical details extending back to Watson-Watt, Wilkins & Bown (1937), who present range–time–intensity (RTI) results from an HF radar with which they identify meteor returns.

Reports of high-altitude optical and radar meteors have been given occasionally for 15 years or more. The optical observations of high-altitude fireballs are the most convincing. Recently, Olech et al. (2013) have described a large Orionid fireball that was observed with

★ E-mail: JDMathews@psu.edu

the Polish Fireball Network of video and photographic cameras. They note a beginning height of 168.4 ± 0.6 km and a terminal height of 69.4 ± 0.6 km with a maximum magnitude of –14.7 ± 1 at 77.7 ± 1.0 km associated with the brightest of four flares. They additionally report a transition from sputtering to ablative processes at an altitude of about 115 km.

Fujiwara et al. (1998) were perhaps the first to unambiguously identify high-altitude meteor events. They utilized both image-intensified TV (IITV) cameras and standard photographic techniques to observe Leonid fireballs in 1995 and 1996. From these, they identified two Leonid fireballs with TV-determined onset heights of approximately 160 km and terminal heights at or just below 90 km, with estimated errors of no more than a few hundred metres. They reviewed earlier publications and noted that IITV camera systems are significantly more sensitive than standard photographic methods and are thus useful for observing meteors at lower luminosity and greater heights than was previously possible.

The observations of Fujiwara et al. were followed by those of Spurný et al. (2000b) who also used photographic and all-sky IITV to observe Leonid fireballs. Betlem et al. (1999) reported solely on the corresponding photographic Leonid results, yielding a stunning contrast. Observing from China during the 1998 shower, Spurný et al. identified 13 high-altitude Leonid fireballs (summarized in their table 2). The all-sky IITV-determined beginning heights of these events ranged from 146 to 199 km. The corresponding photographically determined beginning heights ranged from 116 to 126 km. Ending heights ranged from 73 to 103 km. Nine of the events had all-sky IITV beginning heights clustered near 160 km. During the same campaign, Spurný et al. (2000a) utilized separate narrow field-of-view (FOV; 25° and 25° × 35°) IITV systems, which they refer to as low-light TV (LLTV). These observations yielded seven events with very high beginning altitudes. Of these seven events, three were among those reported in Spurný et al. (2000b) using the all-sky IITV cameras. The greater sensitivity and resolution of the narrow-FOV LLTV system revealed significantly higher beginning heights, as shown in fig. 1 of Spurný et al. (2000a). It is likely to be of great importance to the JRO results presented here that they also report that all of these seven events at high altitudes exhibit 'comet-like diffuse structures' and 'jets' directed more or less perpendicular to the trajectories. Interestingly, three of these events were not considered bright enough to be fireballs.

In light of the above results, Koten et al. (2001) reported that after carefully searching their double-station video data archive, they found three meteor events, two eta-Aqarid and one Perseid, with beginning heights near 150 km, along with a single Lyrid with a beginning height above 130 km. They give the light curves for each of these events, noting the diffuse, intermediate and sharp phases. These phases are now considered to correspond to sputtering and rapid diffusion above and pure ablation below, with the intermediate regime being a mix of the two. While reviewing past observations and the observational convergence towards sensitivity to high-altitude meteors, Koten et al. (2006) significantly extend the prior investigations with a tour de force statistical analysis of 164 meteor events with beginning heights above 130 km. Most of these events were from various Leonid showers, with a few from other showers and with four sporadic meteors. However, their overall data base seems highly biased towards showers. Importantly, they conclude that fragmentation likely plays a significant role in the brightness, and thus observability, of high-altitude optical meteors.

With the convincing evidence of high-altitude optical meteors, we note the relative sparsity of high-altitude radar meteors (HARMs) reported in the literature. Here we seek to understand the reasons for this relative sparsity, and we use radar meteor altitude distributions from various radars as a proxy for all aspects of radar meteor visibility. The earliest radar meteor altitude distribution is that of Hey & Stewart (1947) made in the UK late in World War II using a 55-MHz vertical pointing radar that was likely most sensitive to head-echoes. The peak of the distribution was near 95 km and extended from just below 80 km to just above 120 km. This distribution is given as fig. 2 by Mathews (2004), who also provides a short history of meteor radar. Other early observations include those made from Jodrell Bank in 1952 using both 36.6- and 69-MHz radars. These observations were used to help establish atmospheric density and scaleheights in the meteor zone (Evans 1954) and also pointed to a peak meteor height below 100 km. These and other early distributions are summarized in section 5.6 of McKinley (1961) where his figs 5–13 to 5–16 are of particular interest. Note that all of these early observations were largely of what we now call head-echoes. Thus, the classical 'specular' trail-echo 'ceiling effect' (Mathews 2004) should not have influenced these results; we have not included specular trail-echo altitude distributions as part of this discussion because these are strongly limited by the ceiling effect. However, the ceiling effect is a fine example of where the radio science aspects of radar meteors must be clarified before actual meteoroid processes can be addressed.

In an interesting historical reprise, Hajduk & Hanisko (1997) gained access to the radar data film records from the iconic Springhill Meteor Observatory outside Ottawa, Canada. The 32.7-MHz radar was reported by Hajduk & Hanisko (1997) and Millman (1967) to be high power (2–4 MW, 12 μs pulse, 117 pulses per second) and nearly all-sky because it transmitted from a single half-wavelength crossed-dipole antenna and received on a separate but identical antenna. The Springhill radar is additionally interesting in that it was a high-power but small-aperture (wide beam) radar, and was thus intermediate between the HPLA and LPSA radars mentioned earlier. The data analysed by Hajduk and Hanisko were for the equinox (non-shower) periods of 1957–1967 with some years missing. In his section 4.4, McKinley (1961) reports on the low-power, 'meteor patrol' version of this system. In any case, Hajduk & Hanisko (1997) selected 1609 head-echo meteors from a total of about 25 000 near vernal/autumnal equinox events, and noted that 90 per cent were within the 90–130 km range and were thus at or below an altitude of 130 km. This state of affairs concerning the altitude distribution of radar meteors continued until results from the HPLA radars became available.

As stated above, modern HPLA radar meteor studies began with Chapin & Kudeki (1994a,b), who gave stunning meteor results from the JRO 50-MHz HPLA radar. However, they did not compile an altitude distribution. Such a distribution from JRO is given by Chau & Woodman (2003) who show the statistical parameters, such as the event rate as a function of time and the number of events per altitude bin, for 2002 November 19 (see their fig. 5) during the Leonid shower, as well as the parameters for 2003 February 25 (see their fig. 6), which is a non-shower control date. These altitude distributions show a broad peak centred at 110 km during the shower and an asymmetric narrow peak at ∼113 km for the control date. Chau & Woodman discuss the difficulties in determining head-echo characteristics at JRO where the equatorial electroject (EEJ) often dominates scattering in the meteor zone. Sugar et al. (2010) give altitude distributions for both head- and (range-spread) trail-echoes that are similar to those given by Chau and Woodman.

Pellinen-Wannberg & Wannberg (1994) give an altitude distribution made using the EISCAT 930-MHz radar near Tromso, Norway. Their head-echo distribution peaks near 100 km and falls off rapidly by 110 km. However, they also show a trail-echo distribution that extends from 65 to 165 km. It seems likely that this was actually due to satellites and the space debris range aliased to these altitudes and/or to antenna side-lobe issues. However, this work should be revisited, as confirmed by the conclusion of Vierinen, Fentzke & Miller (2014) concerning side-lobe issues with the 224-MHz radar. Westman, Wannberg & Pellinen-Wannberg (2004) give a comparison of EISCAT UHF (931 MHz) and VHF (224 MHz) altitude distributions, showing the majority of events below an altitude of 100 km with many more VHF events than UHF events. Khayrov (2009) compares the head-echo altitude distributions from the EISCAT Tromso VHF (224 MHz) radar, the UHF (500 MHz) Svalbard Radar (ESR) and the Tromso UHF (930 MHz) radar, and finds peak altitudes below an altitude of 100 km with the UHF distributions somewhat lower than the VHF results. The 932-MHz radar distribution might be lower than the ESR distribution. Khayrov also discusses a few high-altitude events that we return to later.

Mathews et al. (2003) give a meteor altitude distribution made using the Arecibo Observatory (AO) 430-MHz HPLA system with about 2 MW peak power and 0°.17 beam. A few events at altitudes up to about 140 km were seen; however, a 1-ms pulse repetition rate limited unaliased altitudes to less than 150 km. One difference from earlier results was noted, which was that the peak height of the AO UHF meteor distribution was found to be ∼108 km. This is similar to the JRO distribution. This higher peak height was confirmed by Briczinski et al. (2009). Mathews et al. (2008) compared the altitude distributions from the AO (430 MHz), an early (32 panel) version of the Poker Flat Incoherent Scatter Radar (PFISR; 449.3 MHz) and the Sondrestrom (Greenland) Radar Facility (SRF; 1290 MHz). They found the AO distribution to be highest, with the much less sensitive PFISR distribution broadly peaking near 100 km, while the SRF distribution peaks below 100 km. They additionally conclude that sensitivity and radio science (scattering) considerations dominate the observed meteor altitude distribution, which can be thought of as the net meteor observability or instrument function for each radar. Of course, the latitudinal difference in both the atmosphere and the average angle of meteoroid entry in the atmosphere might play a significant role in the meteor altitude distribution pattern that has emerged.

Reports of high-altitude (>130 km) radar meteors are infrequent. Brosch et al. (2001) reported observing 1998 and 1999 Leonid radar meteors at altitudes up to about 400 km using a ∼1 GHz beam-steering military array radar. These observations are widely thought to be of space debris and satellites. Khayrov (2009) notes in his figs 30–39 several meteor events at altitudes up to 218 km. From these figures, it is difficult to judge whether or not these 25 events out of the ∼50 000 meteors during all reported observations are returns from space debris or meteor zone meteors in the antenna side-lobe structure. Brosch et al. (2010) report on high-altitude radar meteors that include 11 meteors with beginning heights greater than 150 km, and one at 247 km, observed using the EISCAT VHF radar. These 11 events were out of a total sample of 22 698 meteors detected in 24 h of observing time, and are convincing from a line-of-sight speed point of view (error levels for Doppler determinations are not given). However, Vierinen et al. (2014) persuasively argues that most, if not all, of these 11 events were in a major, well-documented side lobe of the EISCAT VHF antenna pattern. They demonstrated this result with a set of new observations in which small-range meteors from near-zenith were detected in the relevant side lobe while distant meteors were detected in the main lobe.

It seems evident that while high-altitude optical meteors are well established, the parallel class of radar meteors is not. In fact, it seems likely that the HARM events that have been reported in the literature, and the EISCAT VHF HARM results in particular (Vierinen et al. 2014), are actually side-lobe events. Here, we introduce observations made in 2010 at the JRO that were designed to look for (and we present a case that they have actually found) these HARM events and other meteor-related events, such as fragmentation and flaring, as well as two possible new classes of apparent high-altitude meteor-related events. In discussing the variety of radar signals that appear to be meteoroid-related, we underscore the necessity of understand the scattering process(es) giving rise to these echoes. We describe these radar scattering details in terms of the radio science of the scattering process, and note that when observing radar meteors we have certain advantages over optical observations because the scattering is largely coherent and observed with coherent radar. Earlier interpretations of these details are given in Mathews (2004), Mathews et al. (2010), Malhotra & Mathews (2011), Malhotra et al. (2009), and references therein.

Our companion paper (Gao & Mathews 2015, hereafter Paper II) gives details about our use of satellites to calibrate JRO interferometry and to uncover an error source widely cited as proof of distant side-lobe meteor observations.

2 OBSERVATIONAL SET-UP OF THE JRO

We report results from two sets of 49.92-MHz ($\lambda = 6.0055$ m) radar observations conducted at the JRO from ∼01:00 to 05:00 h (EST) on 2010 April 15 and 16. The JRO antenna is a square array of 18 432 half-wave dipoles ($48\lambda \times 48\lambda$; $\sim 300 \times 300$ m^2) arranged into 64 separate modules of 12 × 12 crossed half-wave dipoles, each enabling two linear polarizations.[1] In turn, 16 modules are combined into a quarter-array that can be individually connected to a transmitter and receiver(s). The full contiguous square array is aligned with one apex-to-apex diagonal, pointed approximately magnetic north–south; the quarter array sections are referred to as north, east, west and south. In our observations, the east and west arrays were used to transmit a linear polarization with 0.55 MW peak power to each array.

The inter-pulse period (IPP) used was 2 ms (300 km aliasing), and 20-μs uncoded pulses were used with 1-μs (150 m) sampling from 75–270 km on a 1-MHz bandwidth. An interferometric receive mode was utilized for both observation sets. On April 15, quarter-arrays north, west and south were used for interferometry, while on April 16, three adjacent and pair-wise orthogonal modules of the south quarter-array were used for interferometry. Complex voltages were recorded to disk for post-analysis. The linear polarization used for both transmitting and receiving is designated north-east (NE). The 3-dB full-width transmit pattern for these observations is about 1°.1 parallel to the magnetic equator and 2°.2 magnetic north–south. The individual (1/64) receive modules have ∼7° beamwidth (∼26 dBi gain) while the individual quarter-arrays have ∼2°.2 3-dB patterns (∼38 dBi). In the various data plots given here, we show the combined transmit–receive patterns. Although not used here, the full array has ∼44 dBi gain.

3 OBSERVATIONAL RESULTS

The two sets of observations discussed here have yielded a wide variety of meteor and meteor-related results. We introduce this event

[1] See jicamarca.ece.cornell.edu/overview.html#radarfacil.

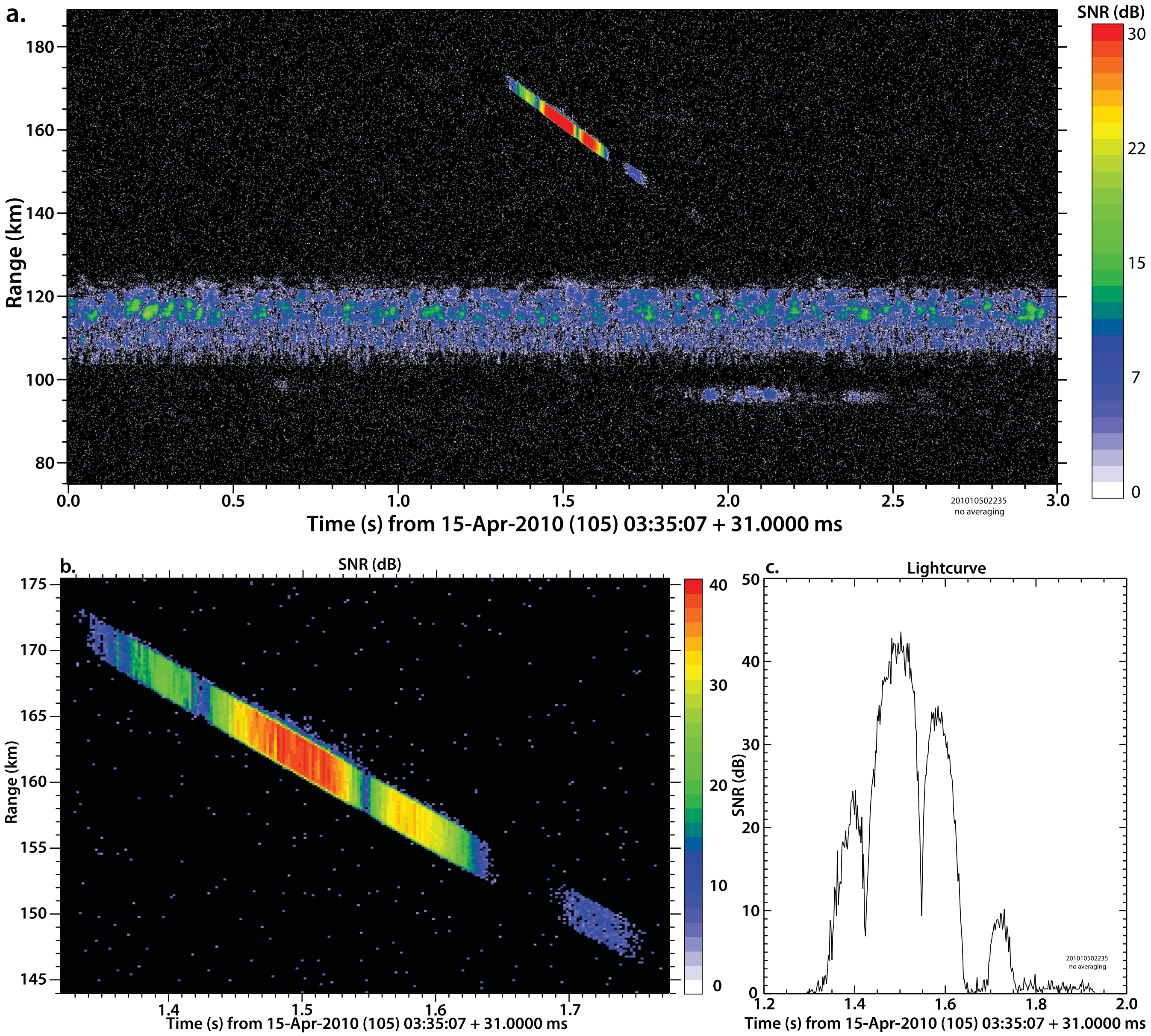

Figure 1. The figure shows a striking 57 km s^{-1} radial speed head-echo event, with small deceleration, that passes through five beam maxima and nulls. This radar meteor clearly has a large scattering cross-section, and interferometry results indicate that the meteor entered the main lobe of the beam. The spacing of the nulls and maxima within the event allow alignment of the event with the beam pattern. Paper II gives details on the JRO antenna calibration, which indicate that this event is at the altitude shown. Note the dynamic range difference between panel (a) and panels (b) and (c). Also note the diffuse event at about 93 km. This is likely the remnant of a ~93-km altitude-narrow sporadic layer that has not been recently recharged with meteor plasma (Malhotra et al. 2008).

set with Fig. 1, which shows the prototype high-altitude event observed on 2010 April 15. While Fig. 1 shows the most compelling example of these events, there are a total of 30 such events on the first night and four on the second night. We define these events as exhibiting head-echoes as opposed to trail-echoes or ill-defined echo types; two other classes of events are also introduced later. In the past, such events have been widely dismissed as being normal meteor-zone events seen in the antenna side lobes. The JRO is a narrow-beam system, and the fact that this event has a high line-of-sight (LOS) speed (~57 km s^{-1}) along with a ~30 km long smooth (little substructure) light curve (Figs 1b and c), showing little evidence of deceleration (<3 km s^{-2}) or of the fragmentation that often occurs in the meteor zone (Briczinski et al. 2009; Mathews et al. 2010; Malhotra & Mathews 2011), further supports our finding that this event did indeed occur at high altitudes rather than in the side lobes at traditional radar meteor altitudes. Note that for the observed high LOS speed, the meteoroid trajectory must be largely radial (towards the radar), which, in turn, implies a shallow trajectory if it is in the beam side lobes. In this case, if we take the centre of the event at 160 km and posit that it is actually at an altitude of 100 km, the trajectory elevation angle is ~39°; we find no relevant antenna side lobes at this angle. We do recognize that the distant side-lobe structure is dominated by array details such as bad array elements. These initial considerations have led us to carefully analyse this and similar events, as thoroughly discussed in Paper II. In particular, the Fig. 1 event shows the meteor passing through four beam maxima and nulls that provide valuable information on where the trajectory is within the beam. Modelling the beam pattern and matching the

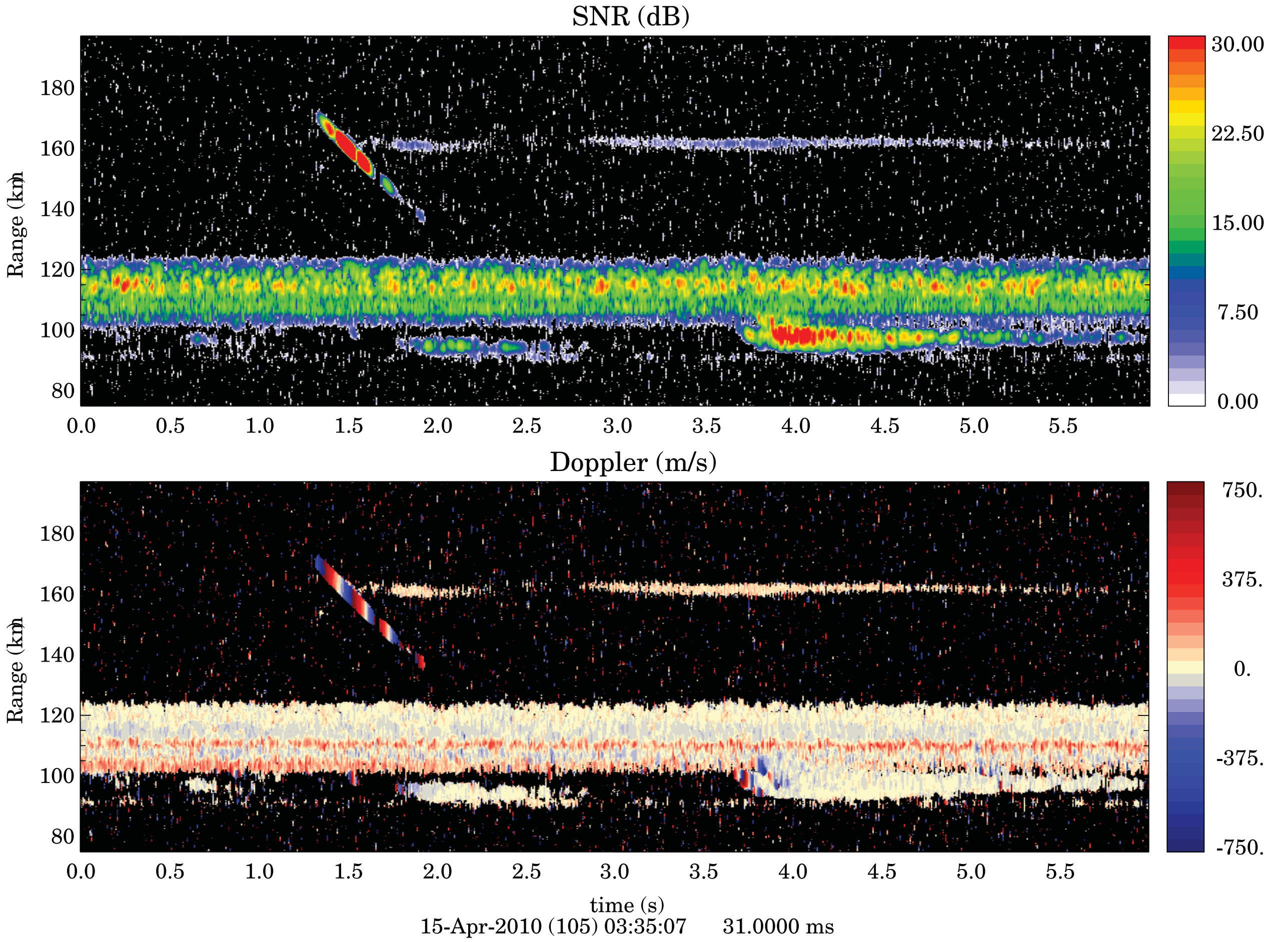

Figure 2. When looking ∼12–15 dB deeper into the noise, the event shown in Fig. 1 also displays a weak trail-echo at **k**⊥**B** nearest the meteoroid trajectory. This trail is consistent with the trail plasma diffusing parallel-**B** to the **k**⊥**B** location yielding coherent scattering over approximately a Fresnel zone. This limits the event to being near the **k**⊥**B** locus, as shown in Fig. 3. Doppler is determined here using pulse-to-pulse correlation that wraps (aliasing) at ±750 m s^{-1}. Thus, meteor head-echoes cycle through all speeds revealing the events centred near 3.75 s and 100 km to be head-echoes followed by RSTEs. Deceleration for this event, while noisy, is <3 km s^{-2}. This deceleration appears to be largely geometric because the angle between the meteoroid trajectory and the radar line-of-sight changes continually.

pattern to the observed pattern for the meteor trajectory are important tools for verifying the meteoroid trajectory within the beam. In this analysis task, the JRO interferometric capability is paramount, as is a careful analysis of the radio science aspects of the event. We conclude that this event likely occurred above the traditional meteor zone and we proceed to carefully examine all of the data in light of this possibility.

The importance of the radio science aspects of the event shown in Fig. 1 for its interpretation becomes clear as we look deeper (∼12–15 dB) into the noise level, as seen in Fig. 2. Fig. 2 shows that this event also produced an altitude-narrow trail-echo that almost certainly comes from the **k**⊥**B** region for the radar. This is the region that produces the long-lived meteor trails often seen at lower altitudes at the JRO (Malhotra et al. 2007b), the Middle and Upper Atmosphere (MU) radar (Zhou et al. 2001), and other radars that see the **k**⊥**B** region. Thus, if this meteor event is in the side lobes, then the trajectory must be largely towards the radar and pass near or through the **k**⊥**B** region in the meteor zone. Of course, this is possible but it is perhaps even more unlikely because this helps to constrain the trajectory to close to the plane of the JRO **k**⊥**B** region. With regards to the last paragraph and Paper II, an examination of the theoretical beam-pattern in the magnetic east–west plane, which contains the antenna centre and has a zenith angle of ∼51° (elevation angle ∼39°), reveals no possible significant side lobe. Again, note that we do not expect the theoretical distant side-lobe pattern to closely resemble the actual pattern that would likely be dominated in the distant side lobes by array irregularities, such as missing elements. However, as noted in Paper II, satellites have not been detected in these distant side-lobe locations.

The phase-unwrapped interferometric pattern for the Fig. 2 trail-echo is given in Fig. 3. This location can be compared with the head-echo trajectory given in fig. 3 of Paper II. As seen in Fig. 3, the phase-unwrapped trail-echo location is consistent with the meteoroid trajectory determined by interferometry as calibrated via the techniques discussed in Paper II.

Fig. 4(a) shows an event similar to the event shown in Fig. 1 that begins at just 140 km. This event has a radial speed of 67.6 km s^{-1}, descends into the traditional meteor zone, and undergoes a terminal flare at an altitude of about 110 km. Thus, the trajectory of this event is much more easily understood interferometrically and the fact that the terminal flare occurs in the traditional meteor zone supports our conclusion that it is not seen in the antenna side-lobe structure. In this case, the relevant side lobes would be different from the event shown in Fig. 1 if it occurred in the distant side lobes. Matching

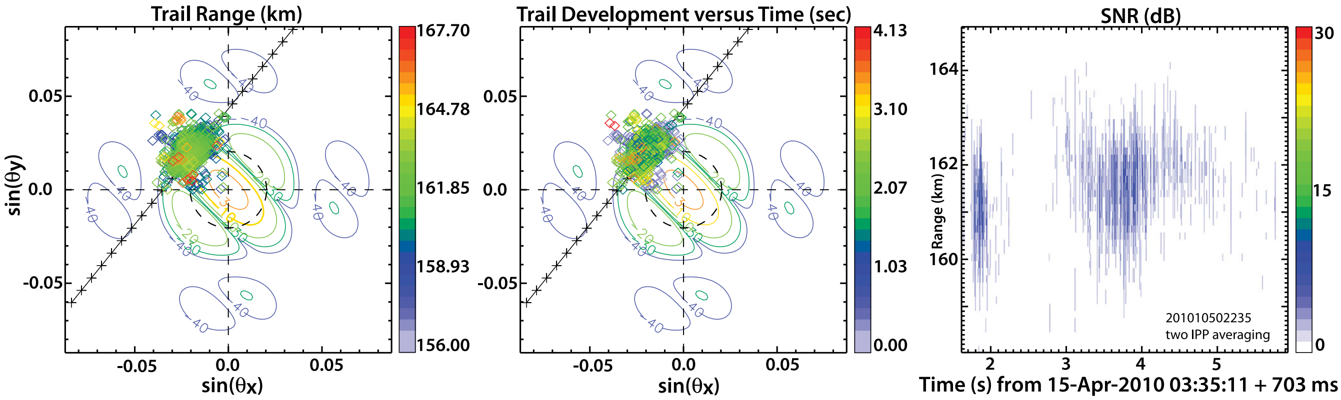

Figure 3. Interferometric location of the trail segments in Fig. 2. The diagonal line shows the location of the **k**⊥**B** region for the JRO located at the centre. The two-way beam pattern is shown in 10 dB increment contours. The circle corresponds to the interferometry phase ($-\pi$,π) ambiguity edge at an altitude of 100 km. The returns are clustered at the edge of the ambiguity circle, consistent with scattering from the **k**⊥**B** region (Malhotra et al. 2007a, b, 2009).

the theoretical beam-pattern with the meteor signal-to-noise ratio (SNR) combined with interferometry reveals that this event is also in the main beam and nearby side lobes. We find that there is a small but statistically important continuum of these head-echo events that have onset heights greater than 130 km. The altitude and altitude-span versus time distribution for these events is given in Fig. 4(b).

Figs 5 and 6 show a pair of instructive meteor events and also demonstrate meteor effects on the lowest scattering (sporadic-E) layer (Mathews 1998; Malhotra, Mathews & Urbina 2008). The 75–97 km meteor event is very complex because it includes head-echoes and multiple trail-echoes, as well as terminal flaring and our first observation of an interference pattern formed between the head-echo and background ionospheric (sporadic-E) scattering layer. The head-echo of this event begins at about 1.15 s and at an altitude of 97 km. Thus, its initial atmospheric trajectory occurred outside the main antenna beam with no hint of it in the nearby side lobes. As the head-echo becomes visible, an immediate RSTE develops, which then completely merges with the 93-km layer by the end of the frame. As the head-echo passes through the range of the low-lying sporadic-E layer, an interference pattern develops, as discussed below. The head-echo intensifies until 90 km, at which point the scattered power decreases abruptly, in a single IPP. The abrupt decrease in scattered power is apparently because of a flare, the result of which appears at 90 km – after 0.5 s (250 IPPs) delay – as a strong scattering layer just below the 93-km sporadic-E layer. The meteor then traverses a minimum in the antenna pattern and, as the scattered power increases, the meteoroid starts to strongly fragment and flare. Fig. 6 shows two details from the full frame shown in Fig. 5.

Fig. 6(a) gives a detail of the low-altitude event show in Fig. 5 as the meteoroid descends from 97 to 86 km and into a beam null. Of particular note is the 93-km low-lying ionospheric layer that is well defined in both Figs 4 and 5 and is weakly present at other times. As the meteoroid passes through the range of this layer, the radar head-echo exhibits an interference pattern that is confined to only the overlapping ranges. This interference pattern also increases in frequency – the rate of change and slope of the fringes – as the meteoroid descends through the layer. The presence of this interference pattern suggests that the 93-km layer is in fact comprised of a single, scattering field-aligned irregularity (FAI; i.e. a well-defined phase centre) over the time-span of the meteoroid transit through the layer. This further suggests that the concept of an ionospheric layer should be re-evaluated, particularly for low geomagnetic latitudes, as we discuss in Section 5.

The head-echo event shown in Figs 5 and 6(a) then intensifies rapidly down to 87 km, at which point the intensity decreases dramatically in a single IPP. Before this point, the intra-pulse and pulse-to-pulse return is relatively smooth, showing little suggestion of an interference pattern that might indicate fragmentation or flaring. After the abrupt decrease in intensity, a mild interference pattern is seen to have developed. This suggests that the meteoroid fragmented and one or more particles flared, leaving at least two particles and resulting in the simple interference pattern (Mathews et al. 2010). The fact that the flare occurred is substantiated by the thin trail-echo that appears at the same altitude at 2 s in Fig. 5. The delay is consistent with a plasma 'blob', generated by the flaring particle, which then diffusively field-aligns until arriving at the **k**⊥**B** region and presenting a substantial scattering cross-section. Note that while the head-echo light curve is consistent with differential ablation (Janches et al. 2009), the appearance of the interference pattern immediately following this event suggests fragmentation and flaring.

Fig. 6(b) shows the final 0.4 s of the meteoroid trajectory in the atmosphere as a radar meteor. The meteoroid again appears to fragment with individual particles flaring, while the head-echo leading edge shows clear deceleration of the remaining, lower mass, particle(s). The fact that multiple particles are flaring at small distances along the trajectory is demonstrated by the range-to-range interference pattern that generates net scattering structures, which vary in range at distances that are small compared with the pulse length. There appear to be at least seven individual flares in the final 0.2 s of this event. This complex terminal flaring structure, apparently due to successive meteoroid fragmentation events, is a common feature in meteors observed at the JRO. It is likely that the approximately **k**⊥**B** geometry renders these events more visible, as discussed later.

The weak high-altitude event shown in Fig. 5 is also quite common in JRO observations. This event appears to be a remnant of a meteor fragmentation–flare event perhaps like that shown at 160 km in Fig. 2. In this case, the head-echo was not seen and likely occurred outside the beam. Alternatively, this event might be the result of a classical tangential-trajectory meteor that, given that the antenna beam is at zenith, is also tangential to Earth. Fig. 7 shows two additional meteor events. The event shown in Fig. 7(a) is a $\sim$46 km s^{-1} head-echo HARM, while the event shown in Fig. 7(b) is likely a classical trail-echo but might be a remnant of a RSTE

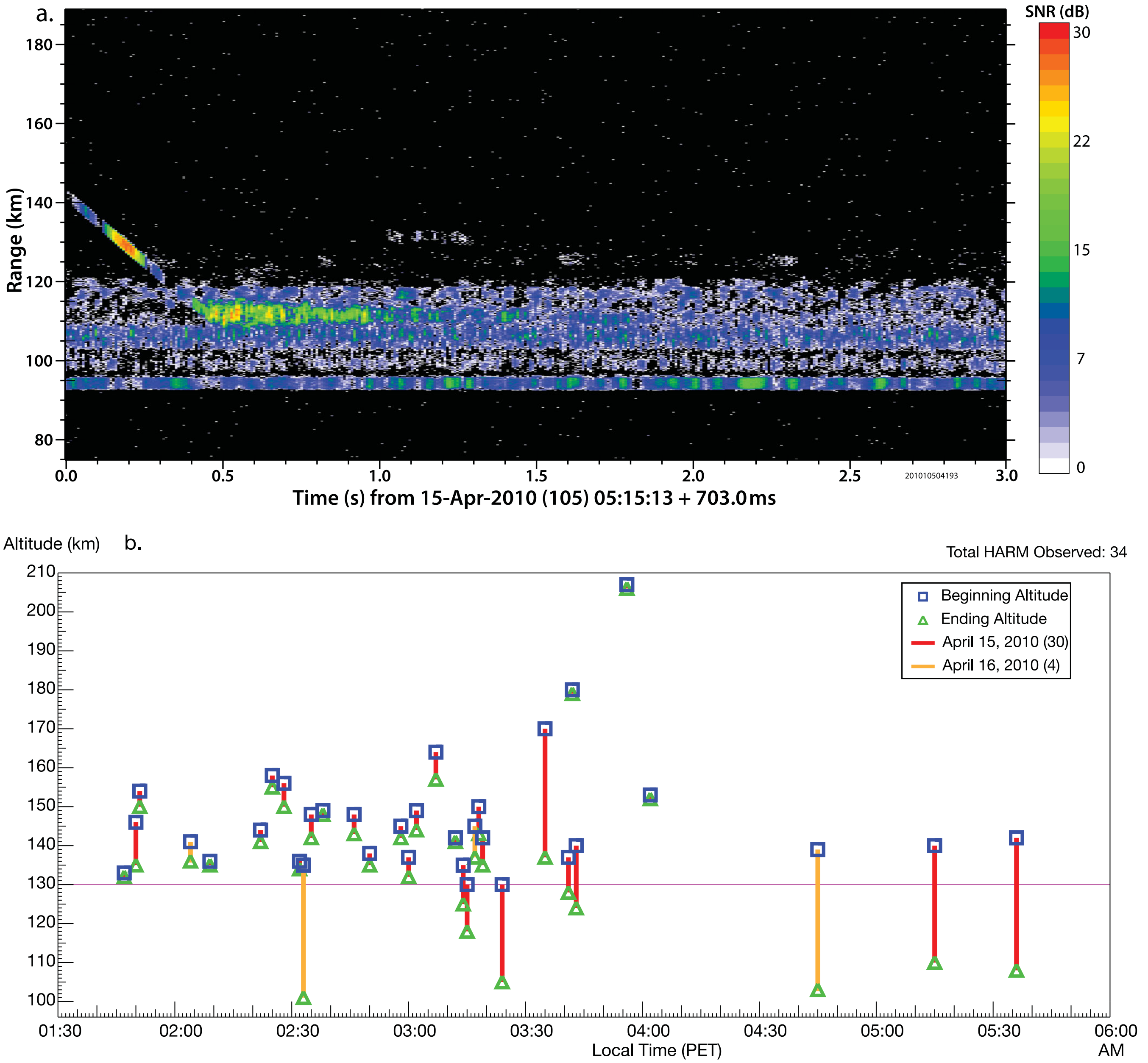

Figure 4. (a) A 67.6 km s^{-1} head-echo meteor event starting just above 140 km and ending in a terminal flare near 110 km. The lowest-lying sporadic-E layer is very altitude-narrow and is apparently sustained all night by direct 'painting' by meteor ionization (Malhotra et al. 2008). The event shown in Fig. 1 and the HARM event shown here are the most compelling of about 34 head-echo HARM events identified in these observations. (b) The altitude and altitude-span versus time distribution of all likely head-echo HARMs identified in these observations. The higher events might be satellites and/or side-lobe events, although they appear to be classical meteors.

like that shown in Fig. 2. Many of the (non-head-echo) HARM events are often best described as amorphous scattering blobs; we thus refer to them here as meteor blob events. That is, we associate the blob events with meteoroids largely because of their highly transient and point-target characteristics. They do not in any way resemble scattering from satellites. Note that we cannot rule out these events as actually appearing in the distant side lobes, especially as these events are so ambiguous in character. However, with regards to our earlier discussions, we believe them to be located near zenith.

The blob events occur often enough that statistical distributions within the beam and with altitude are possible and interesting. The distribution on the sky within the wider beam used on 2010 April 16 shows no particular event affinity to the **k**⊥**B** region, although only 26 events were detected with this wider-beam but less-sensitive interferometry system employed on 2010 April 16. The narrow-beam configuration used on 2010 April 15 resulted in many more events, but the ambiguity width is much smaller and, again, shows no significant clumping with events occurring throughout the ambiguity circle. The blob altitude distributions are given in Fig. 8(b). These distributions underscore the expected difference in the sensitivity between the two interferometry resolutions employed; each receiver was connected to 1/4th of the full array on the first day but to 1/64th of the full array on the second day.

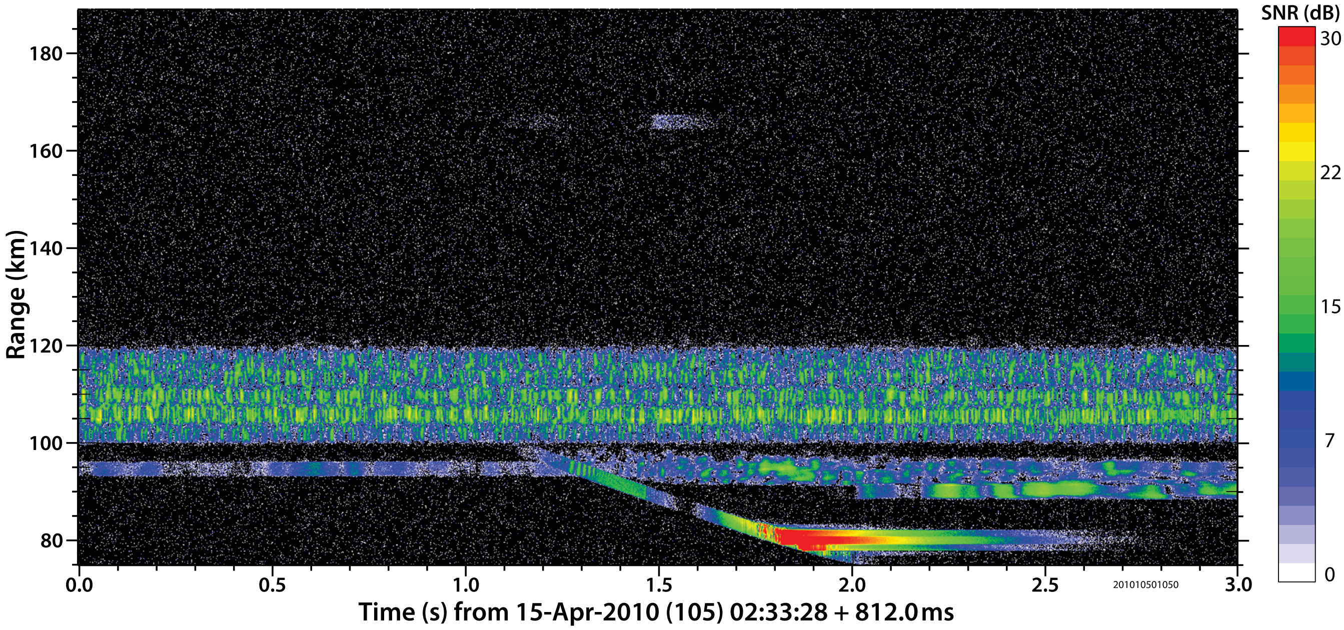

Figure 5. Several radar meteor and meteor-related events typical of the JRO. The 75–97 km low-altitude event has 27.3 km s^{-1} radial speed and shows terminal flaring and several other features discussed in the text. The weak high-altitude blob event is typical for these common features that do not, in general, occur at **k**⊥**B** but typically show sudden onset and slow decay. Note that the 95–120 km FAI scattering zone is largely comprised of thin layers that exhibit pulse-length altitude depth. The lowest layer is altitude-thin and appears to be sustained by meteor events as seen here (Malhotra et al. 2008).

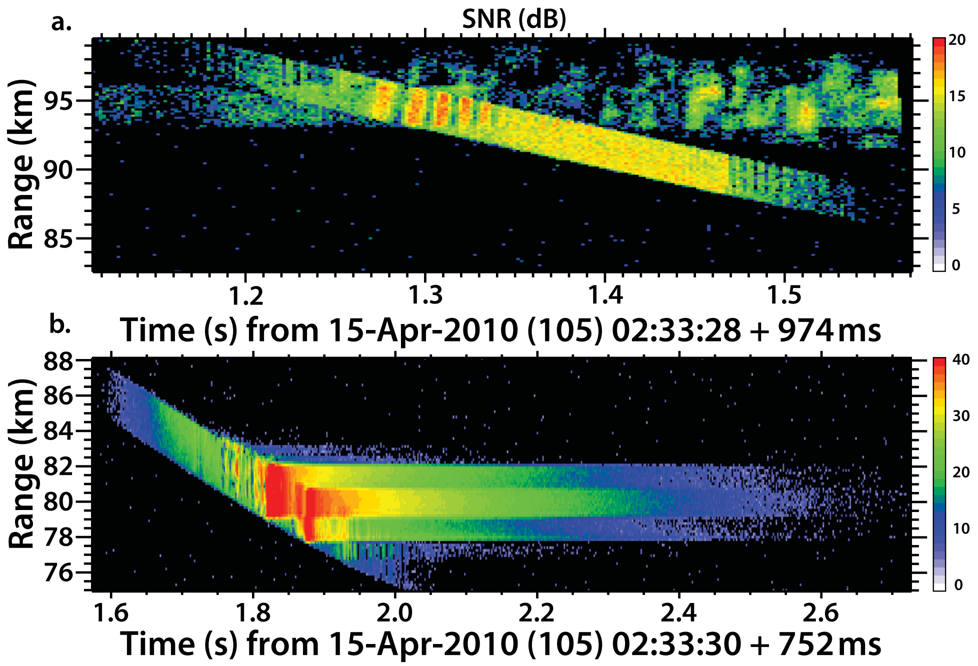

Figure 6. Details from the low-altitude terminal flaring event shown in Fig. 5. (a) The weak 93-km ionospheric layer is shown to be made up of sparse FAI scattering elements, which in this case form a clear interference pattern with the meteoroid head-echo. Note that below 93 km, the head-echo intensifies until abruptly decreasing in strength, followed by a weaker return with a simple interference pattern indicating two major fragments. (b) The meteor head-echo below an antenna pattern null begins to show further fragmentation and flaring as well as deceleration.

The altitude distribution of 2010 April 16 appears to be a sensitivity clipped version of the 2010 April 15 distribution, which in turn is not unlike the distribution of high-altitude optical meteors reported in Spurný et al. (2000a). The low-altitude end of the distribution is ambiguous because of the difficulty in identifying blob events among the increasingly large numbers of normal meteors. The 150-km peak in this distribution is not associated with any antenna side lobe that we can identify. Note that the receive beams are quite different for the two days of observations discussed here.

In Fig. 9, we introduce an apparently unrecognized, likely meteor-related, transient scattering feature associated with the JRO **k**⊥**B**

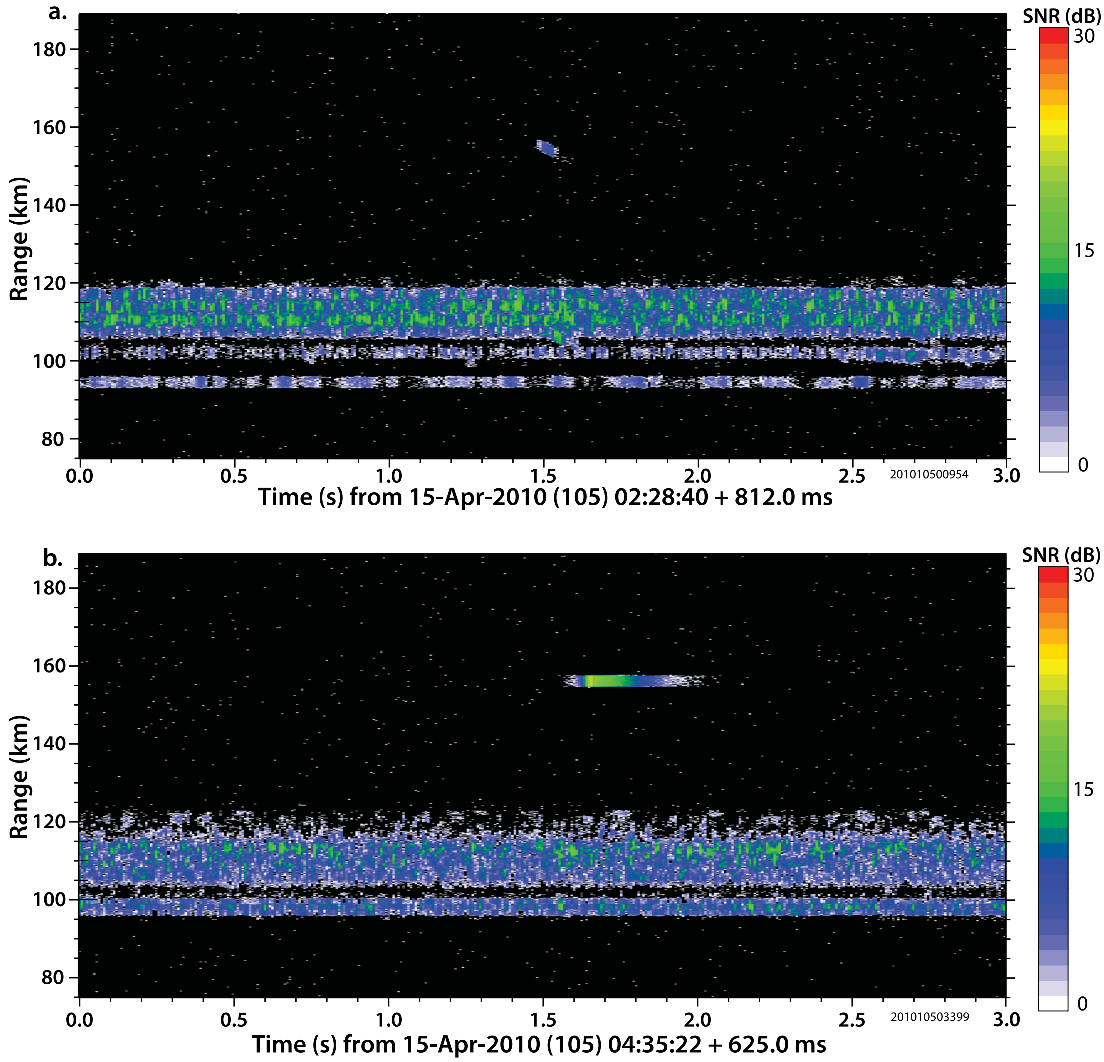

Figure 7. Two typical high-altitude meteor blob events. (a) A very short head-echo with ~46 km s^{-1} radial speed. (b) Likely a classical (trajectory oriented perpendicular to the radar radial) meteor but possibly like the high altitude events of Figs 2 and 5 because it happens to lie at **k**⊥**B**. This is not a satellite return; note the rapid onset and slower decay.

region. We observed 25 of these events – we call them dragons as in the use of 'here be dragons' on ancient maps – during the ~4 h of observing on 2010 April 16 when we used wide-beam interferometry such that the **k**⊥**B** locus was within the ambiguity circle. These generally weak features are also even more weakly observed using the more sensitive but narrow-beam interferometry that placed the **k**⊥**B** locus outside the ambiguity circle; because the narrow receive beam involved a much larger collecting area, the sensitivity at the **k**⊥**B** locus was approximately the same for the two observations. The dragon events mostly extend from the ~125–150 km range, although a few extend up to about the 180-km range. These events resemble the widely discussed (Dyrud et al. 2002; Zhou et al. 2001; Malhotra et al. 2007b; Malhotra et al. 2007a; Malhotra et al. 2009) RSTEs seen in the meteor zone and thus, like HARMS, are suspect as contamination from RSTEs in the side lobes. However, in structure and range extent, these events seem distinct from RSTEs seen in the meteor zone. At this stage, we cannot prove the origin of these events except to say that many appear to show a head-echo-like leading edge and are highly transient, suggesting a meteoroid event origin.

4 DISCUSSION

The goal of the JRO observations described here was to observe in the AO meteor mode, enabling a direct comparison between the two data sets, especially with regard to meteoroid fragmentation and the role of the **k**⊥**B** scattering geometry at the JRO. We also extended the IPP to 2 ms (300 km alias range) from the usual 1 ms, in order to look for the apparent high-altitude meteors seen at the AO. This latter investigation was stimulated by the fact that, as discussed in Section 1, high-altitude optical meteors are well established while the parallel class of radar meteors is not. In examining the excellent JRO data, the event shown in Fig. 1, further explored in Figs 2 and 3, provoked the careful analysis of the JRO beam and of satellite results for evidence of side-lobe contamination. This analysis is presented in Paper II where we find no evidence of side-lobe contamination and considerable evidence supporting HARMs. It is only by employing interferometry in both narrow- and wide-beam modes and by utilizing satellite returns that we come to this conclusion. Having said this, we remain sceptical of the earlier reports of HARM observations as discussed in Section 1. Further, we expect the community to remain cautious

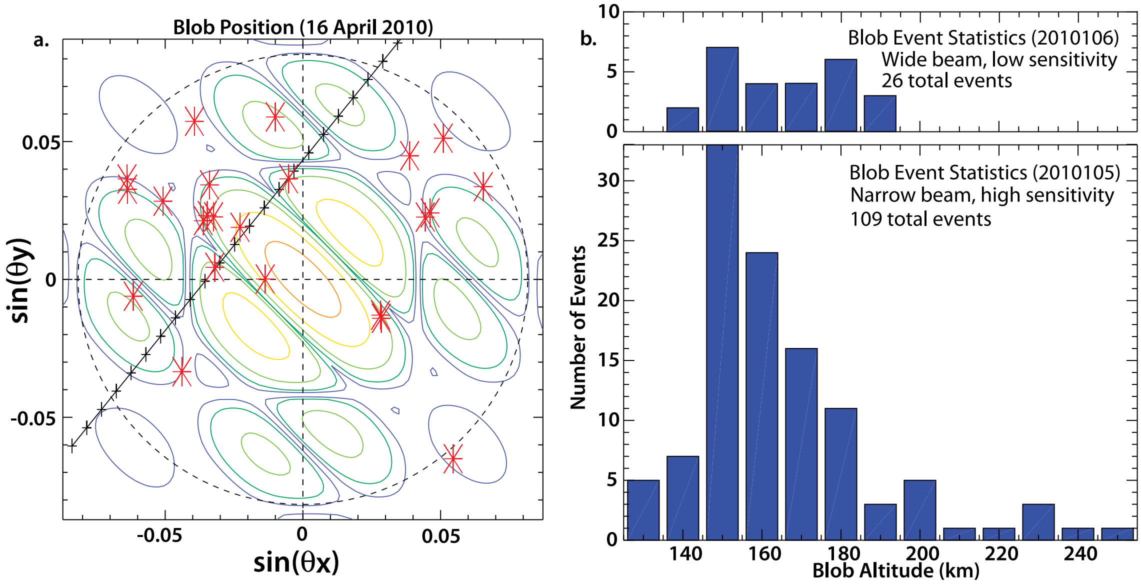

Figure 8. (a) Blob distribution in the beam for all events of 2010 April 16. (b) Blob distribution as a function of altitude for both observation sets. The largest number of events was observed on April 15 where three-quarters of the full array was used for receiving and interferometry, resulting in much higher sensitivity than that for April 16. The April 16 observations were made using three adjacent 1/64 array modules for unambiguous interferometry over a larger area of the sky.

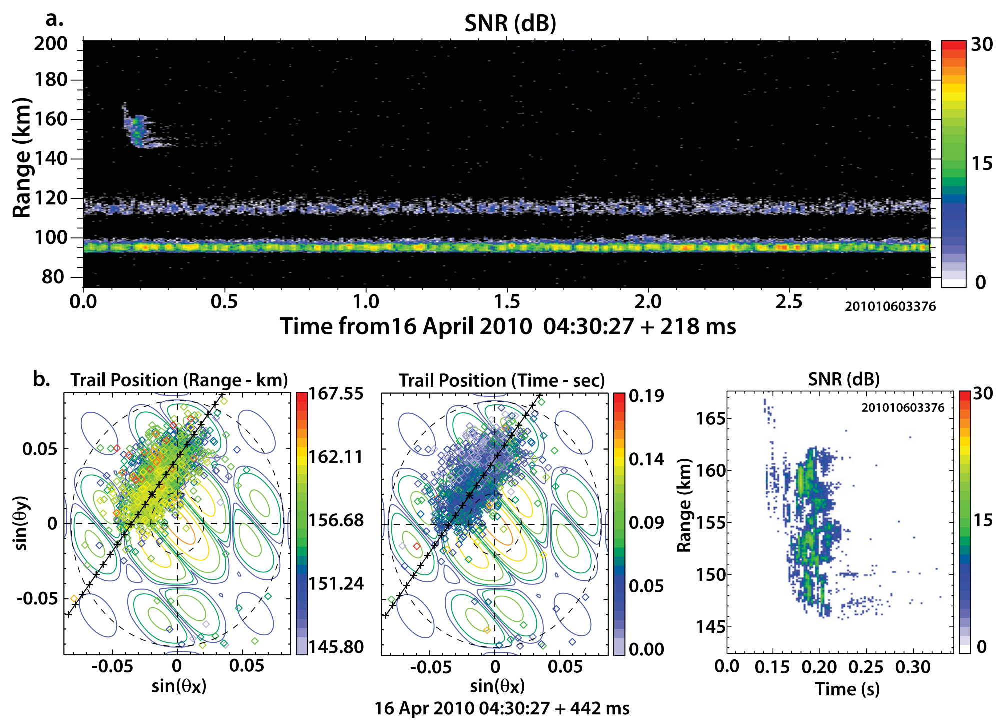

Figure 9. The figure shows a new class of high-altitude, apparently meteor-related, transient radar returns that originate exclusively from the **k**⊥**B** region. We have called these dragon events. (a) An RTI plot showing a dragon event that can be compared with the RTI plots in Figs 1, 2, 4, 5 and 7. These events typically extend 20–30 km in range and are quite distinct from the events shown in the earlier figures. (b) All of the dragon events are seen to be associated with **k**⊥**B** scattering and most show some hint of a head-echo-like leading edge.

concerning the provisional conclusions we have drawn herein. Vierinen et al. (2014) have convincingly demonstrated that a major side lobe in the EISCAT 224-MHz radar resulted in most, if not all, of the high-altitude meteors reported by Brosch et al. (2010). We continue observational attempts to study the JRO side-lobe structure via overt satellite observations and to identify more possible HARMs.

In concluding that the event shown in Fig. 1 was real, we looked for and found, as shown in Fig. 4(b), a continuum of about 30 such head-echo events that display a significant Doppler signature.

Fig. 4 shows an event that begins just above 140 km and ends in a flare with a flare-trail at the 110-km range. The flare occurs in the midst of background scattering layers and so is difficult to study. Fig. 5 – with detailed images given in Fig. 6 – shows a lower-altitude event that is very typical for those observed at the JRO, in that it generates substantial RSTEs and ends with terminal flaring (Malhotra et al. 2007b). This event displayed several fragmentation flares and at least seven terminal flares, all of which emphasizes the need to carefully interpret the radio science aspects of each event. In this case, the interference of scatterers at different ranges shown in Fig. 6(b) is most revealing.

The meteor event shown in Fig. 5 was additionally instructive in that it also revealed that the ionospheric layer it passed through was comprised of a single scattering blob (actually an FAI filament is more likely) with a relatively stationary phase centre that yielded a simple, two-source interference pattern with the head-echo (Mathews et al. 2010). This result highlights the caution we must take when averaging radar returns to better reveal ionospheric layers. These layers, sporadic-E comes to mind (Mathews 1998; Malhotra et al. 2008), might well be comprised of a few individual blobs or filaments that are dispersed in the radar beam and appear as a continuous layer only because of time and/or spatial averaging.

In looking for the rather standard head-echo and HARM events, we discovered a variety of transient events that are sometimes obviously associated with the meteoroid flux to the atmosphere, as well as events that are more difficult to classify. These include the high-altitude blob events, some of which are almost certainly orbital objects but most of which are clearly meteor events that might be HARM events that do not meet our definition, outlined above, of HARMs. The blob events occur throughout the beam and at altitudes up to and even above 200 km. Also included are the dragon events. These are altitude and time extended events that occur exclusively from the $\mathbf{k}\perp\mathbf{B}$ locus at altitudes ranging from 125 to 180 km and that sometimes show a hint of a head-echo. It is possible that dragons are the result of some electrodynamic instability triggered by a meteor. Again, note that we have found no evidence of satellites – which presumably often have Rayleigh-like or even mirror-like radar scattering cross-sections that are much larger than many meteors but are at greater ranges – in the JRO side-lobe structure. This topic is further discussed in Paper II (Gao & Mathews 2015).

In order to better understand the contrast between Rayleigh and meteor (free electron) scattering regimes, we consider three examples. In particular, we note that for the JRO, Rayleigh scattering from a 6.4-cm radius, perfectly conducting sphere is visible at the 100-km range with SNR $\approx$ 1 for 1 MW transmitted power, a mean gain of 41 dBi and a system temperature of 5000 K (a 14.4 cm sphere is similarly visible at the 1000-km range). Coherent (in-phase) scattering from $N = 1.5 \times 10^{11}$ electrons at the 100-km range also yields SNR $\approx$ 1 (Mathews 2004). A 6-cm meteoroid would certainly yield a bolide-class optical signature and would be considered rare. A functioning satellite would be at least metre-scale in size.

As stated in Section 1, the almost complete lack of HARM events in HPLA radar observations is somewhat puzzling, given the solid confirmation of high-altitude optical meteors. Possible explanations include the following.

(i) Collectively, we have all assumed that radar meteors are only seen in the meteor zone, and thus no one has seriously looked for HARMs.

(ii) HARMs have been observed but have been discounted as a side-lobe issue, interference, etc.

(iii) There are true radio science reasons (e.g. an extended plasma resulting in little net scattering; Mathews 2004) that HARMs have not generally been seen.

(iv) There are meteoroid sputtering physics issues that result in little plasma production and thus radar invisibility.

It is likely that at least issues (i)–(iii) are all factors in the paucity or absence of HARM observations. More fundamental issues, such as that outlined in (iv), might play a role. However, we believe that we have observed a variety of HARM returns using the JRO HPLA 50-MHz radar. The high-power JRO 50-MHz radar is ideal for seeing more extended plasmas, and it might well be that $\mathbf{k}\perp\mathbf{B}$ scattering with the plasma confined to the magnetic field flux tubes and rapidly diffusing along them is central to our observing HARMs. We are currently examining AO V/UHF results for additional information on possible HARM events. The fact that interferometry is available at the JRO is an overwhelming advantage in testing for meteor zone events appearing in the antenna side lobes.

5 CONCLUSIONS

One of the most exciting – and widely accepted by the optical meteor community – recent developments in the meteor radar physics community has been the identification of fragmentation signatures in perhaps the majority of meteoroids observed by many of the HPLA radars. The identification of fragmentation has been based on a detailed radio science interpretation of head- and trail-echo scattering properties (Mathews 2004; Kero et al. 2008; Roy et al. 2009; Mathews et al. 2010). Interestingly, discussions of meteoroid fragmentation include the following statement by Levin (1968): "I regard the process of fragmentation of meteor bodies as even more important than is recognized now. Therefore further studies of this process seem to be necessary. It is impossible to predict the course of fragmentation for an individual meteor particle but statistical regularities of the fragmentation process must exist and they should be studied. These statistical regularities are probably somewhat different for different meteor streams and also probably vary with the mass of meteor particles."

We agree with this 45-year-old sentiment.

We further note that Elford & Campbell (2001) reintroduced the subject of fragmentation in concluding that $\sim$80 per cent of the meteors observed by classical HF/VHF LPSA radars, which are ordinarily deemed over-dense, are in fact due to fragmenting meteoroids. Koten et al. (2006) emphasize the importance of fragmentation regarding the brightness, and therefore observability, of high-altitude optical meteors. Fragmentation, or rather evidence interpretable as fragmentation (including complex terminal flaring), is observed in many and perhaps most JRO radar meteors. A more complete understanding of the form – atomic versus smoke or dust (Hunten, Turco & Toon 1980; Hunten 1997) – and physical processes (e.g. ablation versus sputtering) associated with meteoroid flux to the upper atmosphere is critical to understanding the metals aeronomy and electrodynamics of the region (Tong, Mathews & Ying 1988; Morton, Mathews & Zhou 1993; Mathews 1998; Raizada et al. 2004; Plane 2012).

Beyond fragmentation, we have concluded that we observe at least three types of apparent HARM events. These include a few tens each of head-echo, blob and dragon events in $\sim$8 h of observations. The strong head-echo and blob events are likely related, with their relative observability depending greatly on the intrinsic size and speed of the meteoroid as well as the event location in the beam and perhaps relative to the $\mathbf{k}\perp\mathbf{B}$ locus. The dragon events are, we conclude, likely meteoroid-related and might point to meteor-triggered electrodynamics in the night-time upper E-region at the magnetic equator. However, in all cases, we cannot entirely rule out contamination via events seen in the distant side lobes. We live in interesting times.

ACKNOWLEDGEMENTS

We would like to thank Dr Jorge Chau, then Director of Radio Observatorio de Jicamarca, for his help in collecting the data presented here. We thank the JRO staff for performing the observations. The JRO is a facility of the Instituto Geofisico del Peru, operated with support from the National Science Foundation (NSF) grant AGS 09-JRO05448 through Cornell University. This effort was supported under NSF grants ATM 07-21613 and AGS 12-02019 to Pennsylvania State University.

REFERENCES

Baggaley J., 2009, Radio Sci. Bull., 329, 6
Betlem H. et al. 1999, Meteor. Planet. Sci., 34, 979
Briczinski S. J., Mathews J. D., Meisel D. D., 2009, J. Geophys. Res., 114, A04311
Brosch N., Schijvarg L. S., Podolak M., Rosenkrantz M. R., 2001, in Warmbein B., ed., ESA SP-495, Meteoroids 2001 Conference. ESA Publications Division, Noordwijk, p. 165
Brosch N., Haggstrom I., Pellinen-Wannberg A., Westman A., 2010, MNRAS, 401, 1069
Chapin E., Kudeki E., 1994a, Geophys. Res. Lett., 21, 2433
Chapin E., Kudeki E., 1994b, J. Geophys. Res., 99, 8937
Chau J. L., Woodman R. F., 2003, Atmos. Chem. Physics, 4, 511
Dyrud L. P., Oppenheim M. M., Close S., Hunt S., 2002, Geophys. Res. Lett., 29, 8
Elford W. G., Campbell L., 2001, in Warmbein B., ed., ESA SP-495, Meteoroids 2001 Conference. ESA Publications Division, Noordwijk, p. 419
Evans S., 1954, MNRAS, 114, 63
Fujiwara Y., Ueda M., Shiba Y., Sugimoto M., Kinoshita M., Shimoda C., Nakamura T., 1998, Geophys. Res. Lett., 25, 285
Gao B., Mathews J. D., 2015, MNRAS, 446, 3416 (Paper II)
Hajduk A., Hanisko P., 1997, Contrib. Astro. Obser. Skalnate Pleso, 27, 89
Hey J. S., Stewart G. S., 1947, Proc. Phys. Soc. Lond., 59, 858
Hunten D. M., 1997, Icarus, 129, 127
Hunten D. M., Turco R. P., Toon O. B., 1980, J. Atmos. Sci., 37, 1342
Janches D., Dyrud L. P., Broadley S. L., Plane J. M. C., 2009, Geophys. Res. Lett., 36, L06101
Kero J., Szasz C., Pellinen-Wannberg A., Wannberg G., Westman A., Meisel D. D., 2008, Geophys. Res. Lett., 35, L04101
Khayrov T., 2009, MS thesis, Luleå University of Technology
Koten P., Spurný P., Borovička J., Štork R., 2001, in Warmbein B. ed., ESA SP-495, Meteoroids 2001 Conference. ESA Publications Division, Noordwijk, p. 119
Koten P., Spurny P., Borovicka J., Evans S., Elliot A., Betlem H., Stork R., Jobse K., 2006, Meteor. Planet. Sci., 41, 1305
Levin B. Y., 1968, in Kresak L., Millman P. M., eds, Proc. IAU Symp. 33, Physics and Dynamics of Meteors. Reidel, Dordrecht, p. 511
Malhotra A., Mathews J. D., 2011, J. Geophys. Res., 116, A04316
Malhotra A., Mathews J. D., Urbina J., 2007a, Geophys. Res. Lett., 34, L24103
Malhotra A., Mathews J. D., Urbina J. V., 2007b, J. Geophys. Res., 112, A12303
Malhotra A., Mathews J. D., Urbina J., 2008, Geophys. Res. Lett., 35, L15106
Malhotra A., Mathews J. D., Ray K., 2009, Geophys. Res. Lett., 36, L22105
Mathews J. D., 1998, J. Atmos. Solar-Terr. Phys., 60, 413
Mathews J. D., 2004, J. Atmos. Solar-Terr. Phys., 66, 285
Mathews J. D., Briczinski S. J., Malhotra A., Cross J., 2010, Geophys. Res. Lett., 37, L04103
Mathews J. D., Briczinski S. J., Meisel D. D., Heinselman C. J., 2008, Earth, Moon, Planets, 102, 365
Mathews J. D., Doherty J. F., Wen C-H., Briczinski S. J., Janches D., Meisel D. D., 2003, J. Atmos. Solar-Terr. Phys., 65, 1139
Mathews J. D., Meisel D. D., Hunter K. P., Getman V. S., Zhou Q., 1997, Icarus, 126, 157
McKinley D. W. R., 1961, Meteor Science and Engineering. McGraw-Hill, New York
Millman P. M., 1967, in Kresak L., Millman P. M., eds, Proc. IAU Symp. 33, Physics and Dynamics of Meteors. Reidel, Dordrecht, p. 3
Morton Y.-T., Mathews J. D., Zhou Q., 1993, J. Atmos. Terr. Phys., 55, 459
Olech A. et al., 2013, A&A, 557, A89
Pellinen-Wannberg A., 2001, in Warmbein B., ed., ESA SP-495, Meteoroids 2001 Conference. ESA Publications Division, Noordwijk, p. 443
Pellinen-Wannberg A., Wannberg G., 1994, J. Geophys. Res., 99, 11379
Plane J. M. C., 2012, Chem. Soc. Rev., 41, 6507
Raizada S., Tepley C. A., Janches D., Friedman J. S., Zhou Q., Mathews J. D., 2004, J. Atmos. Solar-Terr. Phys., 66, 595
Roy A., Briczinski S. J., Doherty J. F., Mathews J. D., 2009, IEEE Geosci. Remote Sens. Lett., 6, 363
Spurný P., Betlem H., Jobse K., Koten P., van't Leven J., 2000a, Meteor. Planet. Sci., 35, 1109
Spurný P., Betlem H., van't Leven J., Jenniskens P., 2000b, Meteor. Planet. Sci., 35, 243
Sugar G., Oppenheim M. M., Bass E., Chau J. L., 2010, J. Geophys. Res., 115, A12334
Tong Y., Mathews J. D., Ying W-P., 1988, J. Geophys. Res., 93, 10047
Vierinen J., Fentzke J., Miller E., 2014, MNRAS, 438, 2406
Watson-Watt R. A., Wilkins A. F., Bown E. G., 1937, Proc. R. Soc. Lond. A, 161, 181
Westman A., Wannberg G., Pellinen-Wannberg A., 2004, Ann. Geophys., 22, 1575
Zhou Q-H., Mathews J. D., Nakamura T., 2001, Geophys. Res. Lett., 28, 1399
Zhou Q-H., Perillat P., Cho J. Y. N., Mathews J. D., 1998, Radio Sci., 33, 1641

This paper has been typeset from a TEX/LATEX file prepared by the author.